



OPEN

Spin polarized density functional theory calculations of the electronic structure and magnetism of the 112 type iron pnictide compound EuFeAs_2

Farshad Nejdassattari & Zbigniew M. Stadnik

Using density-functional theory, we investigate the electronic, magnetic, and hyperfine-interaction properties of the 112-type iron-pnictide compound EuFeAs_2 , which is isostructural to the high-temperature iron-based superconductor $\text{Ca}_{1-x}\text{La}_x\text{FeAs}_2$. We show that the band structure of EuFeAs_2 is similar to that of the 112-type compounds' family, with hole-like and electron-like bands at the Brillouin-zone center and corners, respectively. We demonstrate that the bands near the Fermi level originate mainly from the Fe atoms. The presence of a mixture of ionic and covalent bonding is predicted from the charge-density and atom-resolved density-of-states calculations. There is good agreement between the calculated hyperfine-interaction parameters with those obtained from the ^{57}Fe and ^{151}Eu Mössbauer measurements. The spatial distribution of atoms in EuFeAs_2 leads to an in-plane 2D magnetism. Moreover, *ab-initio* calculations predict the compound's magnetic moment and the magnetic moments of each constituent atom. Also, the density of states profile provides insight into the relative magnitude of these moments. Electronic structure calculations and Fermi surface topology reveal various physical and chemical properties of EuFeAs_2 . Valence electron density maps indicate the co-existence of a wide range of chemical bonds in this system, and based on structural properties, the transport characteristics are deduced and discussed. A thorough analysis of the atomic structure of EuFeAs_2 and its role in the bond formation is presented.

Recently, the iron-based pnictides containing rare earth (RE) elements have been successfully synthesized, and their electronic and magnetic properties have been extensively studied. Among them, compounds belonging to the family of the 112-type iron-pnictide superconductors $(\text{Ca,RE})\text{FeAs}_2$ (RE = La, Pr, Nd, Sm, Gd) have been widely investigated^{1–5}. In particular, density-functional theory calculations on these class of iron-based pnictides were performed. They suggest the existence of four hole-like and two electron-like bands intersecting the Fermi level (E_F) around, respectively, the Γ and M points, which are related to the Fe 3d and As 4p orbitals¹.

Very recently, a new Eu-containing iron-pnictide compound, EuFeAs_2 , has been synthesized⁶. Its crystal structure is composed of two Eu planes, Fe_2As_2 layers, and zigzag chain layers of As^{2,7}. There are two space groups in which EuFeAs_2 is reported to crystallize. The orthorhombic space group *Imm2* was used in Ref. ⁷, and the monoclinic space group *P2₁/m* was employed in Refs. ^{6,8}.

The presence of Eu and Fe in the EuFeAs_2 compound points potentially towards the existence of rich chemical and physical characteristics. These characteristics can be deduced from the electronic structure and fermiology of this compound. Also, EuFeAs_2 is expected to order magnetically. Indeed, its complex magnetism was studied recently experimentally⁹. However, there has been no first-principles theoretical study of the compound's electronic structure and magnetism.

This work's main objective is to study the origin of some of the physical properties of EuFeAs_2 via a detailed investigation of its electronic structure using the *ab-initio* density-functional theory calculations. The formation and the type of chemical bonds and the charge transport properties in this compound are investigated. The chemical bonds between the various atoms in EuFeAs_2 are found to be similar to those observed in similar compounds^{1,10–14}. A thorough discussion of the Fermi surface topology allows for a better understanding of the electronic characteristics of EuFeAs_2 . A comparison is made between the calculated physical quantities and those

Department of Physics, University of Ottawa, Ottawa, ON K1N 6N5, Canada. email: stadnik@uottawa.ca

obtained from the magnetic and Mössbauer measurements. Moreover, with the aid of *ab-initio* calculations, one can compare the experimental results with those derived from computations.

Theoretical methods

We carried out first-principles calculations of the electronic structure and Mössbauer hyperfine-interaction parameters of EuFeAs₂ in the context of density-functional theory employing the full-potential linearized augmented-plane-wave method that is implemented in the WIEN2k package¹⁵. This method is described in detail in Ref. ¹⁶. In this paper, the interstitial region's valence wave functions are expanded in spherical harmonics up to $l = 4$. They are expanded to a maximum of $l = 12$ in the muffin-tin (MT) region. The MT radii used for Eu, Fe, and As were 2.50, 2.32, and 2.21 a.u., respectively. We used the generalized gradient approximation (GGA) scheme of Perdew et al.¹⁷ for the exchange-correlation potential. For the Eu 4*f* and Fe 3*d* states, the values of the effective Hubbard-like interaction energies of, respectively, 0.55 and 0.20 Ry, were used. For correlated systems and for a full potential calculation, we have used an *effective Hubbard parameter* defined as $U_{\text{eff}} = U - J$. It can be calculated with the augmented plane-wave methods. For the Fe 3*d* states, $U_{\text{eff}} = E_{3d\uparrow}(\frac{n+1}{2}, \frac{n}{2}) - E_{3d\uparrow}(\frac{n+1}{2}, \frac{n}{2} - 1) - E_{\text{F}}(\frac{n+1}{2}, \frac{n}{2}) - E_{\text{F}}(\frac{n+1}{2}, \frac{n}{2} - 1)$, where n is the orbital occupation number¹⁸. A similar relation holds for the Eu 4*f* states. The Hubbard potential of 0.27 Ry with a J constant of 0.065 Ry leads to an effective Hubbard parameter of 0.20 Ry for the Fe 3*d* states. A similar analysis for the Eu 4*f* states leads to the value of 0.038 Ry for the calculated J constant. Combined with the value of 0.59 Ry for the Hubbard parameter, it leads to the effective Hubbard potential of 0.549 Ry (7.48 eV). The plane-wave cut-off parameter was set to $R_{\text{MT}} \times K_{\text{MAX}} = 7.5$. Here, R_{MT} is the smallest MT radius in the unit cell and K_{MAX} is the maximum K vector used in the plane-wave expansion in the interstitial region. One thousand three hundred thirty-one inequivalent k -points were used within a $21 \times 21 \times 21$ k -mesh in the irreducible wedge of the first Brillouin zone. The calculations were done for the experimental lattice and atomic position parameters⁷.

Results and discussion

Crystal structure. The most probable space group in which the EuFeAs₂ compound crystallizes is *Immm*2 (No. 44)⁷. The relevant crystal structure parameters of EuFeAs₂ are given in Table 1.

Figure 1 shows the crystal structure of EuFeAs₂. The interactions between the constituent atoms are shown by the rods connecting these atoms. Each unit cell (Fig. 1a) contains four formula units of EuFeAs₂. The unit cell's dimensions and the atoms' spatial distribution play an important role in the studied compound's electronic properties. The unit cell of EuFeAs₂ is in the form of a cuboid (Fig. 1a), which is highly elongated along the a direction ($a \gg b, c$, Table 1). The FeAs₂ units in each unit cell are greatly separated along the a direction, and, consequently, the interactions are small compared to those along other directions. Moreover, no magnetic coupling is expected to exist along the a direction. Consequently, any possible magnetic order in this compound will be two-dimensional and restricted to the bc plane. The $a \gg b, c$ relationship also indicates that the two-dimensional characteristics in EuFeAs₂ will be more prominent than those in other Fe-based pnictides.

The Fe and As₁ atoms in the unit cell (Fig. 1a) are shown to be connected by thin rods, which represents the covalent bonds within the FeAs₂ units. Covalent bonds within these units are favoured because of the close distance between the Fe and As₁ atoms. The FeAs₂ units are separated by two sheets of the Eu atoms and sheets of the As_{2,3} atoms, which act as insulating layers.

Figure 1b displays multiple unit cells further to indicate the blocks of the FeAs₂ units. The insulating sheets of the Eu and As_{2,3} atoms separating these units are depicted in this figure. One can consider the Eu and As_{2,3} sheets as barriers for the conduction electrons forbidding them to propagate freely along the a direction. The absence of connecting rods between the Eu and As_{2,3} atoms indicates the existence of ionic bonding between them. Consequently, the dominant insulating behaviour of EuFeAs₂ along the a direction results from the formation of ionic bonds to a greater extent and covalent bonds to a lesser extent between the Eu counterions and the Fe-As system.

Based on electron density calculations (*vide infra*), valence charge delocalization is also present between the As₂ and As₃ atoms. Moreover, as the Eu atoms in EuFeAs₂ exist in the divalent state⁹, they transfer their 6*s* electrons to the As_{2,3} atoms and the Fe-As₁ units, thereby forming strong ionic bonds. The Fe-As₁ bond length and the bond angle As₁-Fe-As₁ in EuFeAs₂ are, respectively, 2.4122 Å and 108.212°. It has been suggested that the bond angle correlates with the transition temperature, T_c , in Fe-based superconductors¹⁹. The highest T_c seems to be achieved in the structures with the tetrahedron angle closest to the ideal tetrahedron angle of 109.47°. This suggestion may be consistent with the value of $T_c = 13.8$ K in the EuFe_{0.97}Ni_{0.03}As₂ superconductor^{8,9}.

There is a strong structural similarity between EuFeAs₂ and Ca_{1-x}La_xFeAs₂. The As₂ and As₃ atoms form zigzag chains, and their distances are classified into the short and the long ones. In EuFeAs₂, the short As₂-As₃ distance is 2.5568 Å and the corresponding As₃-As₂-As₃ angle is 99.688°, with the short-distance As₂-As₃ atoms forming one-dimensional zigzag chains along the b direction. The long As₂-As₃ distance corresponds to the interchain distance and is 3.0383 Å. In Ca_{1-x}La_xFeAs₂, the corresponding long and short distances are 2.53 and 3.02, respectively¹. The directional covalent bonds between the As atoms are in a zigzag form.

The complex network of atoms seen in Fig. 1b also appears in other 112-type layered iron-pnictides with the chemical formula RETAs₂ (T = Ag, Au)²⁰. Although the space group *Pmncn* (No. 62) of RETAs₂ is different than those of EuFeAs₂ and Ca_{1-x}La_xFeAs₂, the compound SmAuAs₂ has similar structural Au₂As₂ and As zigzag layers²⁰. In addition, the compound LaAgAs₂, which crystallizes in the space group *Pmca* (No.57), also consists of the Ag₂As₂ and As cis-trans layers²⁰. These As cis-trans chain layers have only recently been discovered in iron-based pnictides⁷. It is feasible that different complex networks of As atoms, because of their 4*p*³ electronic states, can potentially lead to discovering new iron-based pnictides and superconductors.

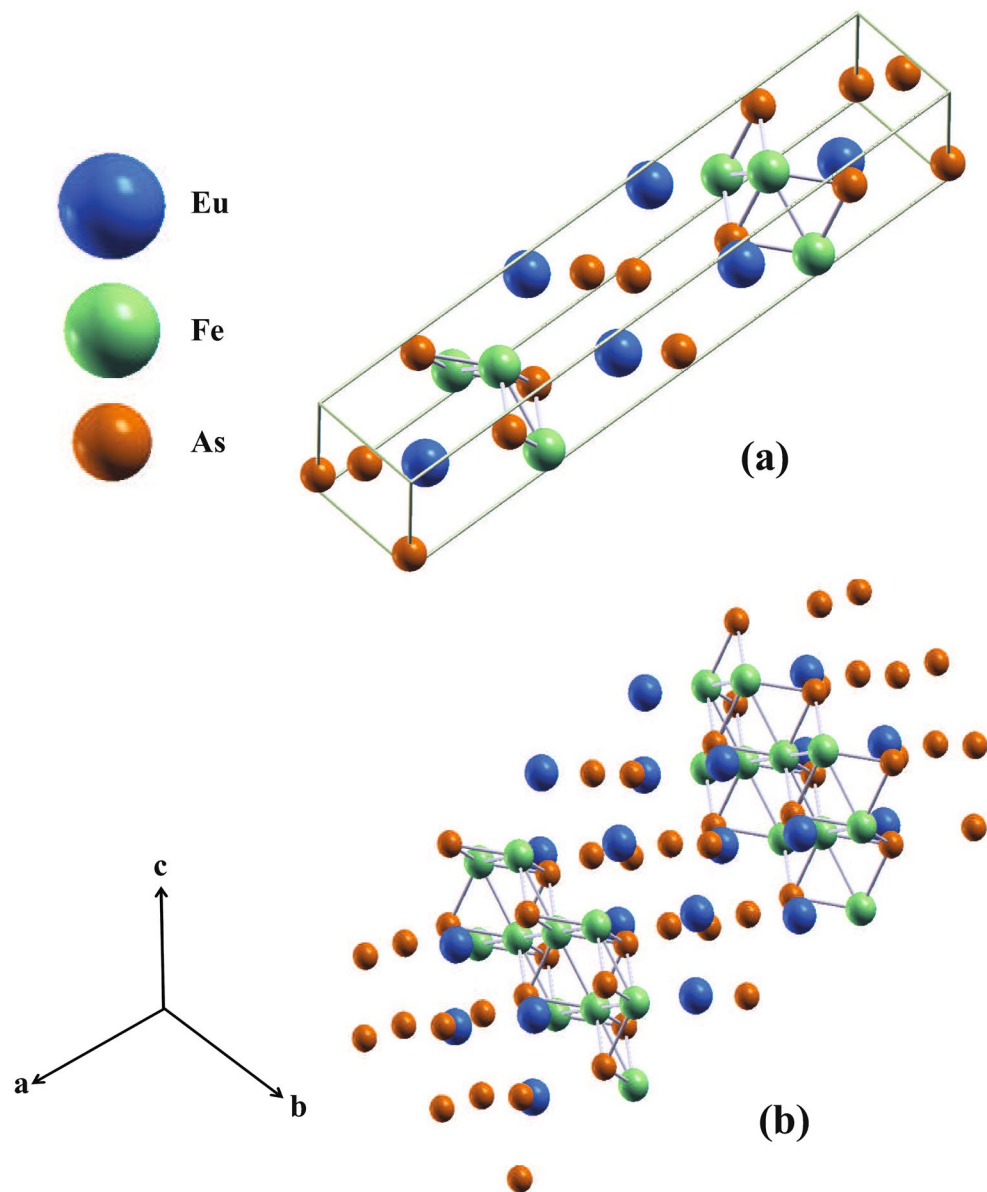


Figure 1. The unit cell (a) and the layered structure (b) of EuFeAs₂. SigmaPlot v14, www.systatsoftware.com.

| Crystal system | | | |
|-------------------------|----------------------|---------------|--------------|
| Space group | <i>Imm2</i> (No. 44) | | |
| <i>a</i> | 21.285(9) Å | | |
| <i>b</i> | 3.9082(10) Å | | |
| <i>c</i> | 3.9752(9) Å | | |
| α, β, γ | 90°, 90°, 90° | | |
| Element | <i>x</i> | <i>y</i> | <i>z</i> |
| Eu | 0.38602 (3) | 1 | 0.75155 (17) |
| As ₁ | 0.31613 (7) | $\frac{1}{2}$ | 0.2521 (6) |
| As ₂ | $\frac{1}{2}$ | $\frac{1}{2}$ | 0.6730 (7) |
| As ₃ | $\frac{1}{2}$ | 1 | 0.2583 (11) |
| Fe | 0.24970 (10) | 0 | 0.2489 (9) |

Table 1. Structural information on EuFeAs₂⁷.

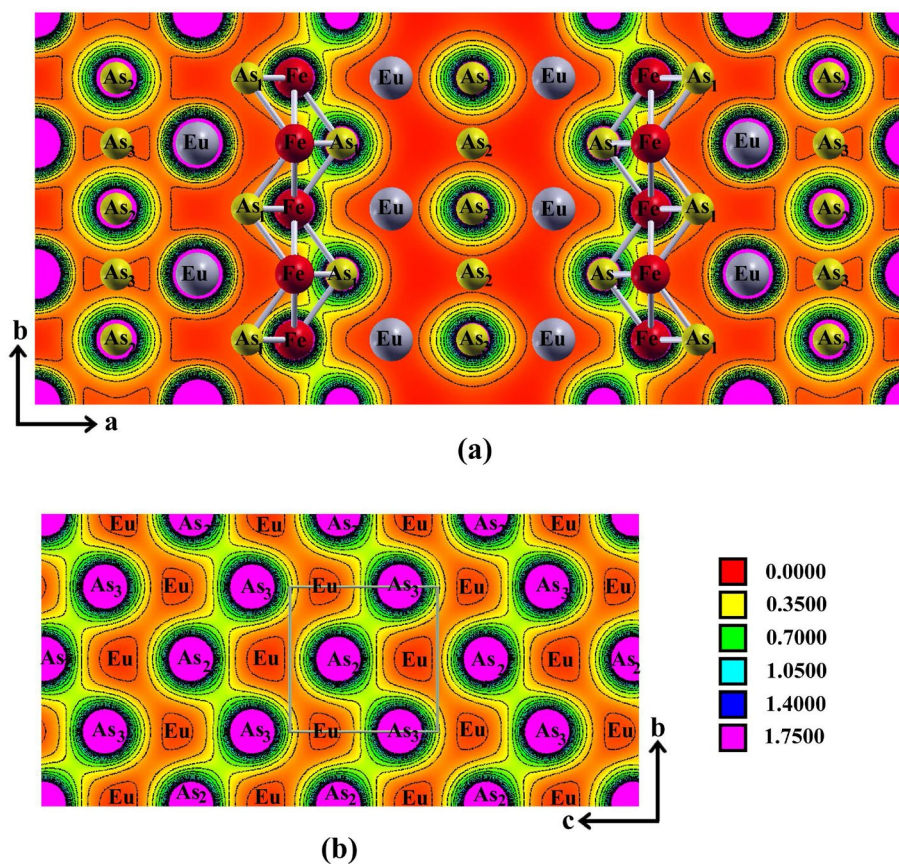


Figure 2. Electron charge density distribution (in units of $e/\text{\AA}^3$) along the (001) (a) and (200) (b) planes. SigmaPlot v14, www.systatsoftware.com.

Valence charge density maps. Figure 2 shows the charge density distributions in the range 0.0–1.75 $e/\text{\AA}^3$ along two crystallographic planes in EuFeAs_2 . The electronic charges are calculated through Bader's analysis scheme²¹. In Fig. 2a, one observes along the elongated direction of the unit cell multiple regions in which the absence of charge density (red regions) is evident. The insulating layers are composed of the Eu atoms blocking any charge transport along the a direction. On the contrary, the chains of the Fe and As_1 atoms form covalent bonds, and thus the regions of higher valence charge density are observed (green regions). This can be related to the Fe $3d$ and As $3p$ hybridization and may indicate that the electric charge transport will, in general, be along these chains.

One also notes (Fig. 2a) that in addition to covalent (directional) bonding between the Fe and As_1 atoms, there are also metallic bonds between two adjacent Fe atoms. They result from the broadening of the Fe $3d$ energy levels near the Fermi level (*vide infra*). These bonds are indicated by the connecting rods in Fig. 2a. Since the Fe atoms do not lie along the (001) plane shown here, the bonds are not shown in the charge density maps. However, this does not indicate that these bonds do not exist. Instead, they are absent in the (001) plane. The charge distribution around the Eu sites and the As_2 sites, in the far left and far right of the unit cell, indicates that the bonding between Eu and As_2 is mainly ionic. In general, the valence charge density distributions indicate the coexistence of ionic bonding (specifically, due to the Eu atoms, and to a lesser extent, the As_2 and As_3 atoms) and covalent bonding (originating from the layers of the Fe and As_1 atoms along the b direction).

In Fig. 2b, the boundaries of the unit cell along the a direction are indicated. One finds that the charge density between the As_2 and As_3 atoms along the b direction is higher than that along the c direction. The reason for this can be traced back to the insulating role of the Eu atoms. This suggests covalent bonds between the As_2 and As_3 atoms. The valence states of both atoms are s -type and p -type, indicating the possibility of forming directional bonds. The presence of such bonds in the zigzag chains of the As_2 and As_3 atoms was also found from the analysis of the synchrotron X-ray diffraction spectra of $\text{Ca}_{1-x}\text{La}_x\text{FeAs}_2$ ¹. The color contour maps in Fig. 2b clearly show the charge density distributions of regular zigzag As chains. The $4p$ orbitals between As_2 and As_3 overlap, forming the directional bonds in the zigzag chain. In contrast, there are no significant charge densities between the interchain As atoms, which indicates the absence of chemical bonds. Even stronger arguments regarding the type of chemical bonds based on the calculated density of states are given later (*vide infra*).

As mentioned above, Eu in EuFeAs_2 is in the divalent state^{9,22}. The charge density maps indicate the electronic charge transfer from the Eu to the Fe-As layers. In other words, the ionic bonding is the consequence of this transfer, resulting in the Eu^{2+} and $[\text{FeAs}_2]^{2-}$ ions. One may also interpret this result by comparing the relatively

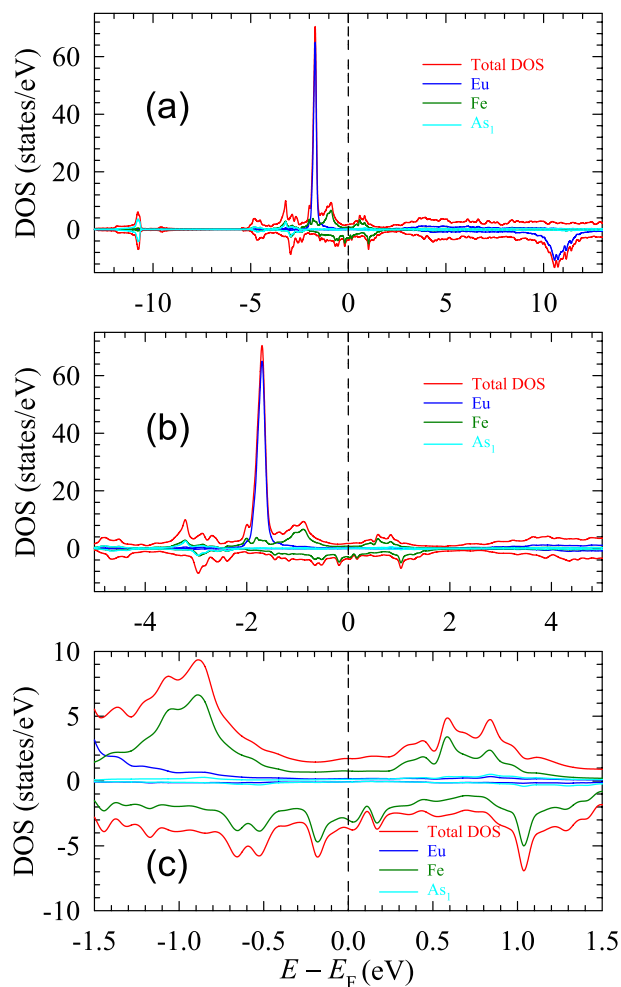


Figure 3. Spin-resolved, total and atom-resolved DOS in EuFeAs_2 for the energy range between -13 and 13 eV (a), -5 and 5 eV (b), and -1.4 and 1.4 eV (c). SigmaPlot v14, www.systatsoftware.com.

large differences in the electronegativities of the Eu (1.2) and the As (2.18) and Fe (1.83) atoms. Likewise, the formation of covalent bonds between the As and Fe atoms results from their similar electronegativity values.

With the above valence charge transfer analysis, one may express the chemical formula EuFeAs_2 as $\text{Eu}^{2+}(\text{Fe}_2^{2+}\text{As}_2^{3-})_{1/2}\text{As}^-$. The first of the two Eu 6s electrons is transferred to the Fe–As₁ layer and the other to the As zigzag layer. Two Fe 4s electrons, together with a single Eu 6s electron, are transferred to the Fe–As₁ layer. Their related orbitals overlap with three empty As₁ 4p orbitals, shaping covalent bonds in the Fe–As₁ layers.

The As zigzag bond layers are composed of As[−] ions with the 4p⁴ electronic states. Because the crystal field around the As ions is anisotropic, the threefold degeneracy of the As[−] 4p orbitals is expected to be removed. The As₂ and As₃ ions are closely packed along the *bc* plane. This causes the *p_x* orbital with two electrons to become stabilized due to the large spatial overlap. In contrast, the *p_y* and *p_z* orbitals with one unpaired electron become destabilized due to their small overlap. The latter two orbitals spread along the *bc* plane, forming the 45° angles with the *b* and *c* directions. Thus, one predicts that the zigzag pattern is formed by directional bonding between the As₂ and As₃ atoms in close proximity.

Density of states. Using density functional theory, we investigate the electronic, magnetic, and hyperfine-interaction properties of the 112-type iron-pnictide compound EuFeAs_2 .

We performed density of states (DOS) calculations using the modified tetrahedron method²³. Figure 3 shows the spin-resolved, total and atom-resolved (except for the As₂ and As₃ atoms) DOS of EuFeAs_2 . The DOS calculated over the wide energy range is displayed in Fig. 3a. One observes a sharp peak at -1.7 eV, which originates from Eu's majority spin states. These Eu 4f states are highly localized as their energy width is small. The Eu's minority spin states, on the other hand, peak at around 10.5 eV. Although they are broader than the corresponding majority spin states, they are nonetheless confined to an energy interval 9.5–11.7 eV. The energy difference between these two spin states results from the large value of the effective Hubbard parameter (7.48 eV) used for Eu, which shifts the minority spin states out of the Fermi energy region. Since these minority spin states (spin-down states) lie high in energy, no electron can potentially be excited into them. Consequently, they remain empty and play no role in the physical properties of the compound studied.

| Number of states at the Fermi level | Spin up | Spin down |
|-------------------------------------|---------|-----------|
| $N(\text{EuFeAs}_2)$ | 1.81626 | 3.74682 |
| $N(\text{Eu})$ | 0.22862 | 0.00282 |
| $N(\text{Fe})$ | 0.80444 | 2.98899 |
| $N(\text{Fe } 3d)$ | 0.34999 | 1.54276 |
| $N(\text{Fe } d_{z^2})$ | 0.07564 | 0.37144 |
| $N(\text{Fe } d_{x^2-y^2})$ | 0.07564 | 0.15241 |
| $N(\text{Fe } d_{xy})$ | 0.07564 | 0.37144 |
| $N(\text{Fe } d_{xz})$ | 0.01693 | 0.15241 |
| $N(\text{Fe } d_{yz})$ | 0.10500 | 0.37144 |
| $N(\text{As}_1)$ | 0.14352 | 0.06732 |
| $N(\text{As}_2)$ | 0.04445 | 0.05461 |
| $N(\text{As}_3)$ | 0.04445 | 0.05461 |

Table 2. The total and partial DOS (in states/eV) in EuFeAs₂.

By comparing the Eu's majority and minority spin state DOS (Fig. 3a), one finds a large difference between the maximum DOS for these two components (Table 2). This difference leads to a relatively large magnetic moment of 6.9 μ_B carried by the Eu atoms.

The calculated DOS allows one to deduce qualitatively the nature of chemical bonding in which the Eu atoms participate. Because the overlap region (Fig. 3a) of the Eu DOS with the DOS of Fe and As is small (due to its highly localized DOS profile), one can speculate that the Eu atoms participate in forming ionic bonds with the Fe and As atoms and to a lesser extent weaker covalent bonds. This agrees with the earlier conclusion that was based on the electron charge density distributions. Also, one can see that the Eu DOS is negligible at E_F and in the E_F region. Therefore, one expects part of the insulating properties of EuFeAs₂ to emerge from the lack of Eu f states in the Fermi region.

The Fe DOS spans the region from -3.5 to 1.8 eV (Fig. 3b). It originates mainly from the Fe $3d$ states, which are relatively delocalized in energy and dominate the E_F region. Therefore, the electrical properties of EuFeAs₂ can be related to these states. The Fe spin-up states peak at -3.2 , -1.7 , -0.9 , and 0.6 eV, whereas the spin-down states peak at -0.6 , -0.2 , and 1.0 eV. The DOS profiles of the Fe spin-up and spin-down states are asymmetric both in the number of states (Table 2) and in the location in the energy spectrum, which explains the nonzero Fe magnetic moment ($0.78 \mu_B$). A careful inspection of Fig. 3b shows a relatively large energy gap in the spin-up states and a pseudogap in the spin-down states across the E_F region.

A closeup plot of the DOS in the E_F region is shown in Fig. 3c. One can notice that the DOS in the vicinity of E_F , although very small, originates mainly from the Fe states. The spin-down Fe states show a minimum slightly above E_F (at 0.1 eV), similar to what is observed in other Fe–As containing compounds^{24,25}.

Figure 4a displays the spin-polarized, total and orbital-resolved DOS of Fe in a wide energy range between -13 and 13 eV. One notices that the Fe $3d$ states dominate the DOS in the E_F region. In Fig. 4b, we examine the spin-polarized DOS of the five orbitals of the Fe $3d$ states. The maximum peak in the spin-up DOS at -0.9 eV arises mainly from the d_{z^2} , $d_{x^2-y^2}$, d_{yz} , and d_{xy} states. The d_{xz} orbital contributes to the DOS mainly above E_F . The states originating from this orbital lead to the peaks in the spin-up DOS at -2.0 , 0.6 , and 1.0 eV. The d_{z^2} states, together with the d_{xz} states, give rise to the DOS in the vicinity of E_F . Most of the electronic properties of EuFeAs₂ result from them. Close to the semi-core energy region (between -3.2 and -2.9 eV), one finds peaks arising from the d_{xy} and d_{yz} orbitals.

The spin-polarized DOS of the As atoms located at three crystallographic positions (Table 1) is shown in Fig. 5. It is evident that the dominant contribution to the DOS comes from the As₁ atoms. The deep core states, which are the atomic-like states, peak at -10.7 eV. They do not contribute to the physical and chemical properties of the compound studied. One observes two peaks (Fig. 5): one at -3.2 eV from the spin-up states, and the other at -2.9 eV from the spin-down states. These peaks coincide with the Fe peaks deriving from the d_{xy} and d_{yz} orbitals (Fig. 4b). There are two smaller peaks in the vicinity of E_F (Fig. 5) at -0.9 and 0.8 eV. They also overlap with the peaks of the Fe d orbitals. These overlaps can explain the chemical bonding between the Fe and As₁ atoms, thus confirming the earlier conclusion based upon the electron charge density maps and the structure of the EuFeAs₂ compound. Moreover, it can also be seen (Fig. 5) that the DOS stemming from the As₂ and As₃ atoms completely overlaps with each other throughout a wide energy range, and its contribution to the total As DOS is minute. This significant amount of overlap over a wide energy range is the signature of covalent bonding between the two As atoms because such states are highly delocalized in energy. This observation confirms an earlier conclusion based on the analysis of the charge density maps (Fig. 2b).

As mentioned earlier, the As₂ and As₃ atoms do not form bonds with the Fe atoms. The absence of such bonds can be partially due to a large separation between these As and Fe atoms. Therefore the hybridization between these As atoms and the Fe–As₁ layers is negligible, as observed from the DOS plots.

Another important feature of Fig. 5 is the near-perfect symmetry of the spin-up and spin-down DOS profiles. This accounts for the near-zero magnetic moment of the As atoms in the compound studied. For regions above E_F (typically above 2.0 eV), the As atoms' DOS profile is similar to that of a quasi-free electron gas. This similarity is mainly because these states are related to conduction bands, and because of their high energy, they are unoccupied. In Table 1, the values of the contributions to DOS of various atoms and orbitals are given.

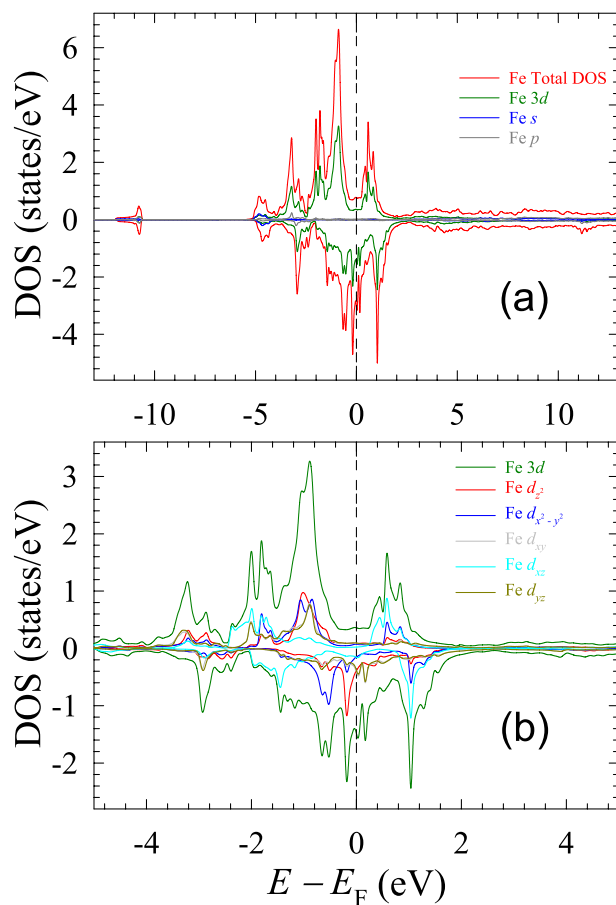


Figure 4. Spin-resolved, Fe total and orbital-resolved DOS (a) and Fe d -orbital-resolved DOS (b). SigmaPlot v14, www.systatsoftware.com.

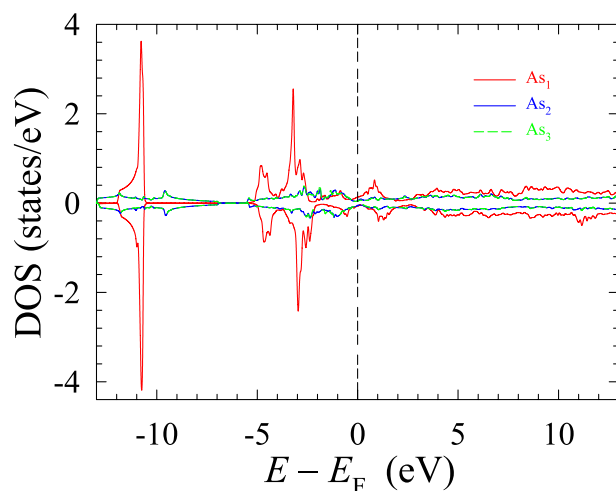


Figure 5. Spin-resolved DOS of As. SigmaPlot v14, www.systatsoftware.com.

Energy band structure. The spin-resolved energy band structure of EuFeAs₂ is presented in Fig. 6. It is plotted along the k -paths passing through high symmetry directions in the conventional Brillouin zone shown in the middle of the figure. One notices in Fig. 6a that there is a dense concentration of nearly flat bands around 1.7 eV. These bands are related to the strongly localized Eu $4f$ states. As one moves in the Brillouin zone from one symmetry point to another, they show almost zero dispersion. As the effective mass m^* of the carriers is inversely proportional to the band curvature, $m^* \sim [\nabla_{\mathbf{k}}^2 E(\mathbf{k})]^{-1}$, the electrons in these localized states cannot participate

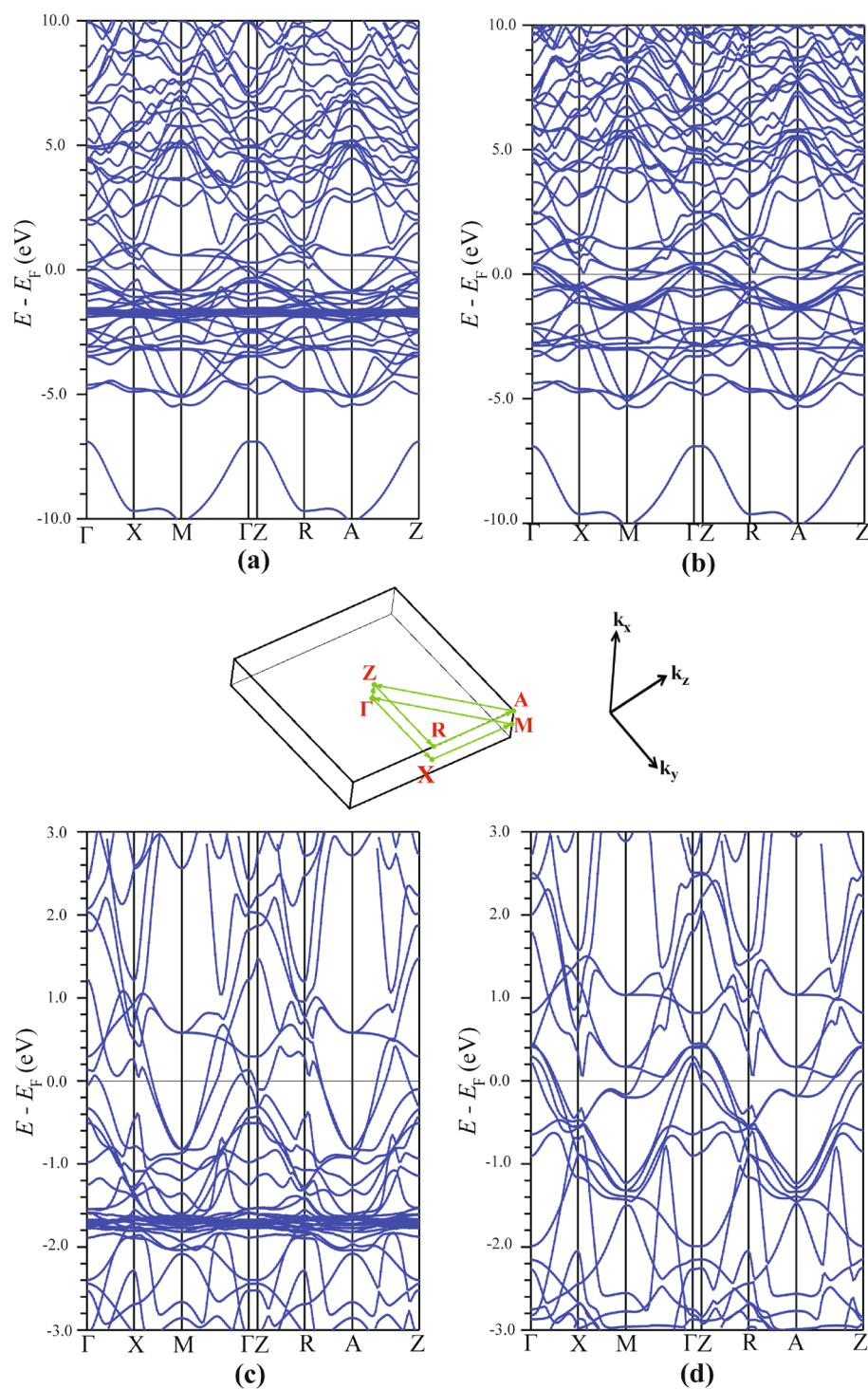


Figure 6. Spin-polarized band structure of EuFeAs₂ in the high-symmetry directions of the conventional Brillouin zone. The spin-up (a) and spin-down (b) band structure in the energy range between -10 and 10 eV. The spin-up (c) and spin-down (d) band structure close to the Fermi level. The \mathbf{k} -paths along the high symmetry directions are shown in the middle of the figure. SigmaPlot v14, www.systatsoftware.com.

in transport properties, and are essentially immobile. The numerous packed bands arising from the Eu $4f$ states verify the presence of a very high DOS peak in Fig. 3a.

Another feature of the band structure (Fig. 6) is the presence of a highly dispersive region extending from ~ 2 eV to higher energies. All bands in this region are the practically empty conduction bands. Their large

dispersion indicates that they are of the s and p character and mostly derive from the Eu and As atoms. Below E_F (Fig. 6a), and except for the flat Eu bands, one finds a region of less dispersive bands. These bands are primarily related to the Fe and As₁ states. Between -5 and -4 eV (Fig. 6a), a couple of energy bands are observed, which arise from the As semi-core states. Below -5 eV, a large gap separates the semi-core bands from a single-core band lying deep in energy.

Figure 6b is the spin-down counterpart of Fig. 6a. Its features are similar to those of Fig. 6a discussed above. There are, however, some differences. First, the spin-down Eu $4f$ states are pushed, due to the large Hubbard parameter, far above the E_F region to energies higher than 10 eV. Second, several energy bands are crossing E_F . They originate from the Fe $3d$ states, in agreement with the results from the DOS calculations (Fig. 3a).

As the energy band structure, and the DOS, in the proximity of E_F determine most of the physical and chemical properties of the compound, we display the spin-up and spin-down energy band structure of EuFeAs₂ in the energy range between -3 and 3 eV in Fig. 6c,d, respectively. These band structures show some features also observed in other Fe-based pnictides^{26–30}. However, there are some differences. There are four hole-like bands at $\Gamma(0,0)$ (Fig. 6d): one peak at 0.2 eV, the next one at 0.3 eV, and the two other bands become degenerate and peak at 0.4 eV. This is different from what was found for such a pnictide as BaFe₂As₂, where three hole-like bands appear near the Γ point³¹. Two electron-like bands at point M(π,π) are seen in Fig. 6c, which is similar to what is observed in another Fe-based compound LaFeAsO³¹. This figure also shows that the two electron-like bands merge at points M and A, where the Brillouin zone is highly symmetric, and thus the states become degenerate at these points. As one moves away from these high-symmetry points, the bands start to diverge from each other. The hole-like band around the highest symmetry point Γ is also seen to cross the E_F .

One notices in Fig. 6d that the number of bands crossing the E_F is larger than for the spin-up case (Fig. 6c). Moreover, in both figures, the highly dispersive conduction bands above 1 eV can be clearly seen, in contrast to the less dispersive Fe $3d$ bands dominating the E_F region (between -1 and 1 eV).

Similar to other Fe-based pnictides, the electronic structure of EuFeAs₂ is mainly determined by the Fe-As layers. There is, however, a distinctive difference between the band structure of EuFeAs₂ and that of other known Fe pnictides. Figure 7 depicts the spin-resolved energy band structure along the \mathbf{k} -path $\Gamma - \Sigma - N - \Sigma_1 - Z - \Gamma - X$ in the first Brillouin zone. There are very few dispersive bands crossing E_F . Qualitatively, the same feature observed in Fig. 6 can also be seen in the band structure along this other \mathbf{k} -path. An important observation here is that the hole-like bands are concentrated along the Γ direction. In contrast, the electron-like bands are found around the N and X directions. Since a few bands crossing the Fermi level (Fig. 7), one may conclude that insulating properties of EuFeAs₂ are more dominant than the conducting ones. Thus, one can categorize EuFeAs₂ as an insulator or a weak conductor.

Figure 8 shows the weighted Fe and Eu energy bands. The thickness of the bands represents their "weight" in the Brillouin zone. It is clear that the E_F region is dominated by the Fe bands originating from the $3d$ states and that Eu $4f$ bands do not appear in this region. Therefore, one can state that the Fe $3d$ bands essentially determine the physical and chemical properties of EuFeAs₂.

The spin-resolved energy band structure of the five Fe $3d$ orbital-resolved states is shown in Fig. 9. All Fe bands are depicted as "thick" bands in other bands' background (the band thickness indicates its relative weight with respect to the overall band structure of EuFeAs₂). The spin-up portion of the d_{z^2} band (Fig. 9a) lies below E_F , whereas the spin-down portion crosses E_F at mid-point along the $\Gamma - X$, $Z - \Sigma_1$, and $\Gamma - \Sigma_1$ directions. The contribution from the d_{z^2} orbital to the band crossing of E_F is almost negligible (Fig. 9c,d). The bands associated with the d_{xz} orbitals (Fig. 9g,h) are somewhat away from E_F . The bands originating from the d_{yz} orbital (Fig. 9i,j) are degenerate with those emerging from the d_{z^2} orbital at the Γ and Z points.

Fermi surface topology. Among the numerous energy bands in EuFeAs₂, only a few contribute to the Fermi surface, and the majority of the energy bands show negligible dispersion at the Fermi level.

As has been observed in the previous sections, the electronic properties of EuFeAs₂ depend predominantly on the electronic structure in the E_F region. In particular, the energy bands and occupied states in the proximity of E_F determine most of the compound's electronic transport properties. This highlights the importance of the fermiology of the compound. The Fermi surfaces (or Fermi sheets) are branes in the reciprocal space that separate the unoccupied states from the occupied ones and constitute constant energy (the Fermi energy) regions. Most properties of a compound stem from the size and shape of these surfaces.

Figure 10 displays the spin-resolved Fermi surface sheets in the primitive Brillouin zone together with the corresponding band structures in the neighbourhood of E_F . Qualitatively, the resulting surface topology agrees with the band structure calculations. For the spin-up case, one observes the presence of a hole-like band in the center of the Brillouin zone along the $Z - \Gamma$ path (Fig. 10b) corresponding to the Fermi sheet in the central region (Fig. 10a). Moreover, as one moves along the $\Gamma - X$ direction, a hole-like and two electron-like bands cross E_F (Fig. 10b) and the emerging Fermi sheets are shown at the corners of the Brillouin zone (Fig. 10a). One observes two electron pockets along the four corners of the Brillouin zone. Along the $\Gamma - \Sigma - N$ path, the hole-like sheets (Fig. 10a) corresponding to the hole-like bands (Fig. 10b) can also be seen.

Figure 10c,d show the spin-down Fermi surface topology and the energy bands, respectively. The hole-like sheets along the $\Gamma - X$ and $Z - \Gamma$ directions can be observed in Fig. 10c. These sheets correspond to the hole-like bands in Fig. 10d. A close inspection of Fig. 10c,d shows that starting from the Γ point and moving towards the Σ point, the first two hole surfaces related to the two hole-like bands (which peak at 0.2 and 0.3 eV) are in a shape of an oval and a square cylinder, respectively. The two nearly degenerate hole-like bands located midway along the $\Gamma - \Sigma$ path correspond to the two barely resolved adjacent hole-like sheets (Fig. 10c). By careful comparison of these Fermi surfaces with the Fe orbital-resolved bands in Fig. 9, one concludes that by traversing the Brillouin zone from Γ to Σ , the four sheets described above derive from the Fe d_{xy} , $d_{x^2-y^2}$, d_{yz} , and d_{z^2} orbitals, respectively.

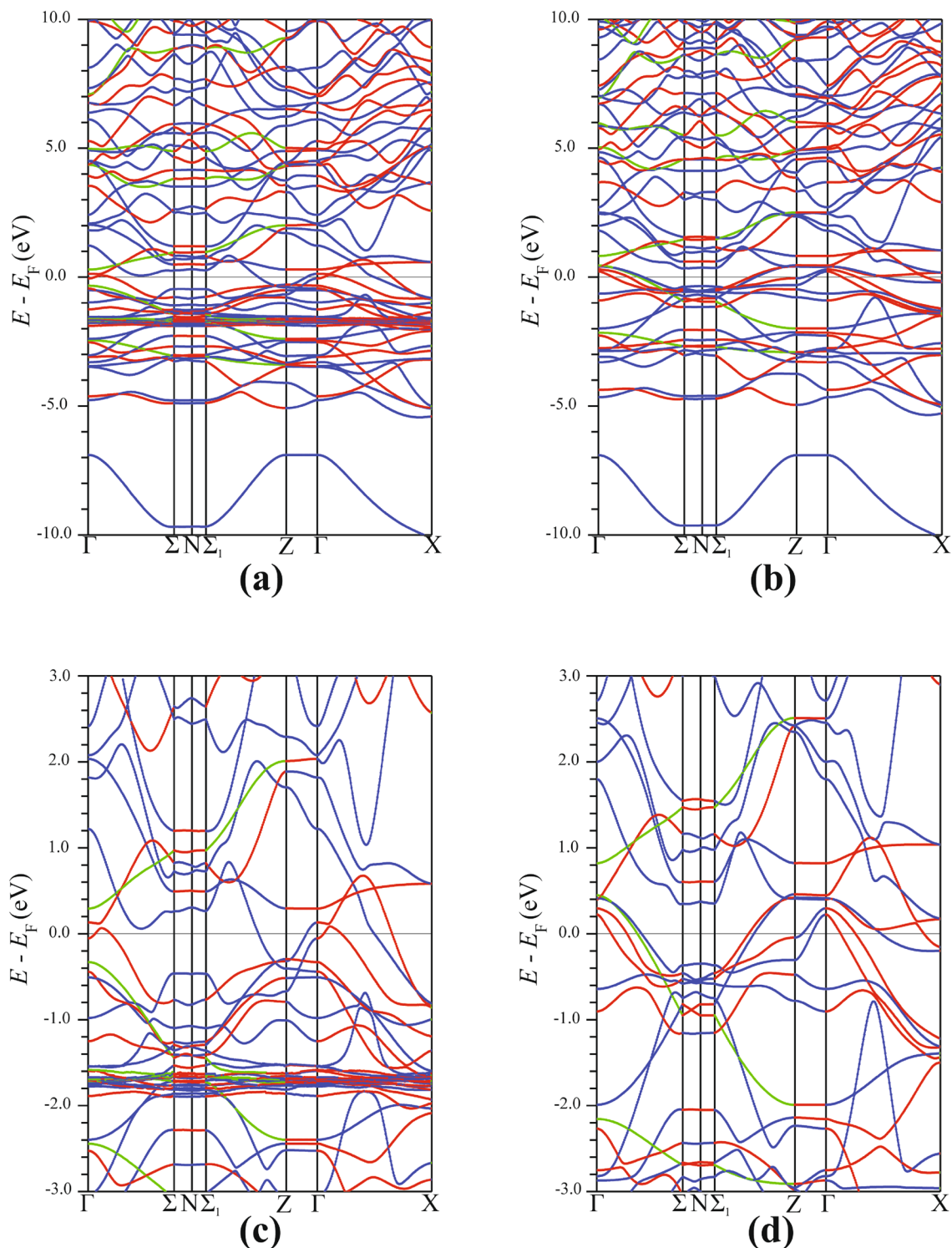


Figure 7. Spin-polarized band structure of EuFeAs₂ in the high-symmetry directions of the conventional Brillouin zone. The spin-up (a) and spin-down (b) band structure in the energy range between -10 and 10 eV. The spin-up (c) and spin-down (d) band structure close to the Fermi level. SigmaPlot v14, www.systatsoftware.com.

Magnetic moments and Mössbauer hyperfine parameters. Each formula unit of EuFeAs₂ contains two Eu atoms, two As₁ atoms, one As₂ atom, one As₃ atom and two Fe atoms. The calculated magnetic moments are listed in Table 3. The total magnetic moment per formula unit ($15.43822 \mu_B$) consists of the contribution from the muffin-tin region ($15.16166 \mu_B$) and that from the interstitial region ($0.27656 \mu_B$). The calculated mag-

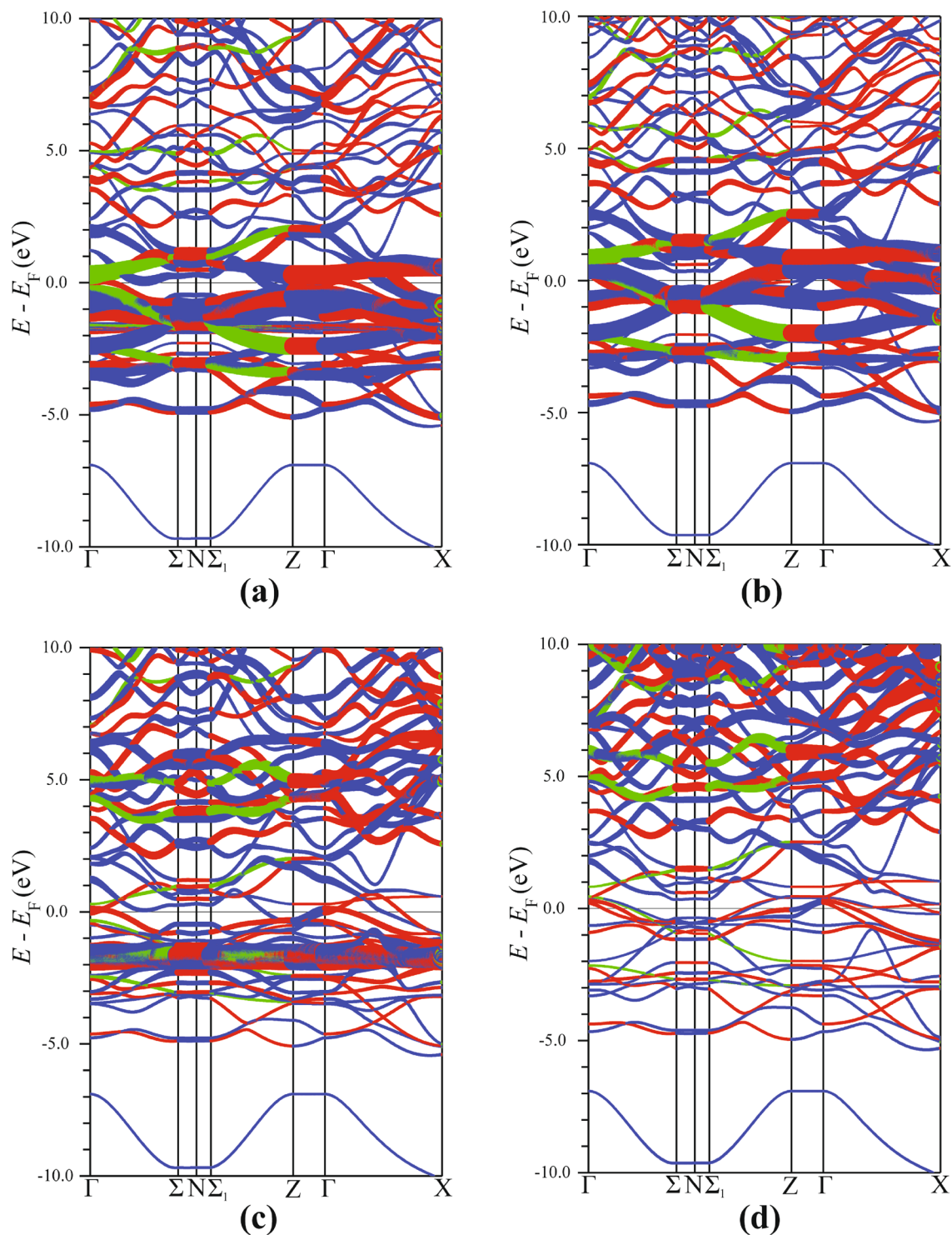


Figure 8. Spin-polarized, weighted energy band structure of EuFeAs_2 . The spin-up (a) and spin-down (b) band structure of Fe. The spin-up (a) and spin-down (b) band structure of Eu. SigmaPlot v14, www.systatsoftware.com.

netic moment of Fe ($0.78029 \mu_B$) is in excellent agreement with the experimental value of $0.78(1) \mu_B$ estimated from the Mössbauer data⁹. It is evident (Table 3) that the dominant contribution to the magnetic moment of EuFeAs_2 derives from the Eu atoms.

We note here that the studied compound crystallizes in the $Imm2$ space group, whereas the majority of iron-based pnictides crystallize in the $P2_1/m$ space group. The $Imm2$ space group can result in relatively localized magnetic moments, which are usually robust. On the other hand, the $P2_1/m$ space group can lead to very itinerant magnetism in iron-based pnictides, making the calculated magnetic energies extremely sensitive to

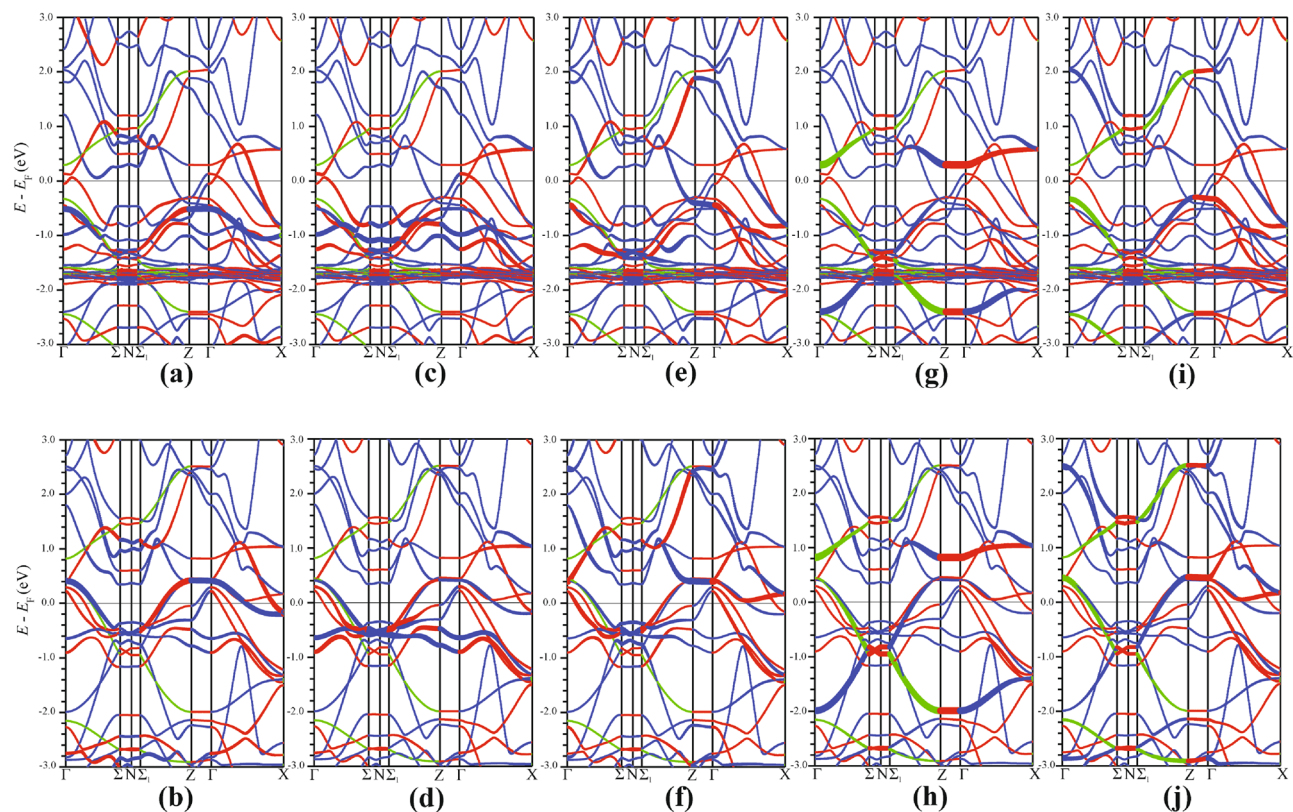


Figure 9. Spin-polarized, Fe 3d orbital-resolved band structure shown by weighted bands in the background of the EuFeAs₂ energy bands. The d_{z^2} contribution to the spin-up (a) and spin-down (b) energy bands. The $d_{x^2-y^2}$ contribution to the spin-up (c) and spin-down (d) energy bands. The d_{xy} contribution to the spin-up (e) and spin-down (f) energy bands. The d_{xz} contribution to the spin-up (g) and spin-down (h) energy bands. The d_{yz} contribution to the spin-up (i) and spin-down (j) energy bands. SigmaPlot v14, www.systatsoftware.com.

the type of approximations used in the DFT calculations. It is also known that GGA calculations increase the tendency towards magnetism as they underestimate spin fluctuations. We have not optimized the lattice and atomic position parameters for the current compound but used their experimental values. There are studies that relate the bonding angle between the As and Fe atoms in the Fe layers to the Fe magnetic moment³². It seems that the 108.212° bonding angle may be a factor leading to a relatively small Fe magnetic moment in EuFeAs₂.

Calculations carried out for antiferromagnetic configurations, where the Eu magnetic moments are confined to the b - c plane and change direction along the alternating layers along the a direction, show an increase in the Fe magnetic moment. This magnetic moment is ~ 1.8 and $\sim 2.1\mu_B$ for the antiferromagnetic checkboard and stripe configurations, respectively.

To understand the magnetic interactions in the Eu layers of the compound studied, we apply an effective Heisenberg model, $\hat{H} = J_1 \sum_{\langle i,j \rangle} \mathbf{S}_i \cdot \mathbf{S}_j + J_2 \sum_{\langle i,j \rangle} \mathbf{S}_i \cdot \mathbf{S}_j$. Here $\mathbf{S}_i(\mathbf{S}_j)$ is the spin of the Eu atom identified by $i(j)$ and the summation is over nearest neighbors. The first term with the coupling constant J_1 indicates interactions between the in-plane Eu atoms, while the second term with the coupling constant J_2 describes interactions between the Eu atoms along the a direction. The calculated values for J_1 and J_2 are 89 μRy and 6.6 μRy , respectively. Also, the calculated values for the Fe-Eu nearest-neighbor interactions give a coupling constant of 82 μRy for the d - f exchange interaction. Using the 108.212° bonding angle between the As and Fe atoms in the Fe layers, we calculated the Fe layers' spin exchange to the nearest-neighbor and next-nearest-neighbor to be 2.2 mRy and 0.7 mRy, respectively. The calculated magnetic exchange interaction between Fe nearest-neighbor atoms is 65 mRy.

We also calculated three hyperfine-interaction parameters, which can be derived from the Mössbauer spectra. These parameters are the isomer shift δ_0 , the hyperfine magnetic field H_{hf} , and the principal component of the electric field gradient tensor V_{zz} ^{33,34}.

The isomer shift is calculated from the following relation: $\delta_0 = \alpha[\rho(0) - \rho_{\text{ref}}(0)]$. Here, $\rho(0)$ and $\rho_{\text{ref}}(0)$ are, respectively, the total electron densities at the Mössbauer nucleus in the compound studied and in the reference material, and α is a calibration constant. To account for the possibility of the penetration of the $p_{1/2}$ electrons into the ⁵⁷Fe nuclei, relativistic spin-orbit effects were included in the calculations of ρ ³⁵. As a reference material for ⁵⁷Fe Mössbauer spectroscopy, α -Fe metal (with the bcc structure and the lattice constant of 2.8665 Å) was used. The calculated values of $\rho(0)$ and $\rho_{\text{ref}}(0)$ were found to be 15308.415 and 15309.918 (a.u.)⁻³, respectively. With the calibration constant $\alpha = -0.291(\text{a.u.})^3(\text{mm/s})$ ³⁶, these ρ values lead to $\delta_0 = 0.4374 \text{ mm/s}$. The calculated δ_0 is in fair agreement with the experimental value of 0.547(2) mm/s⁹.

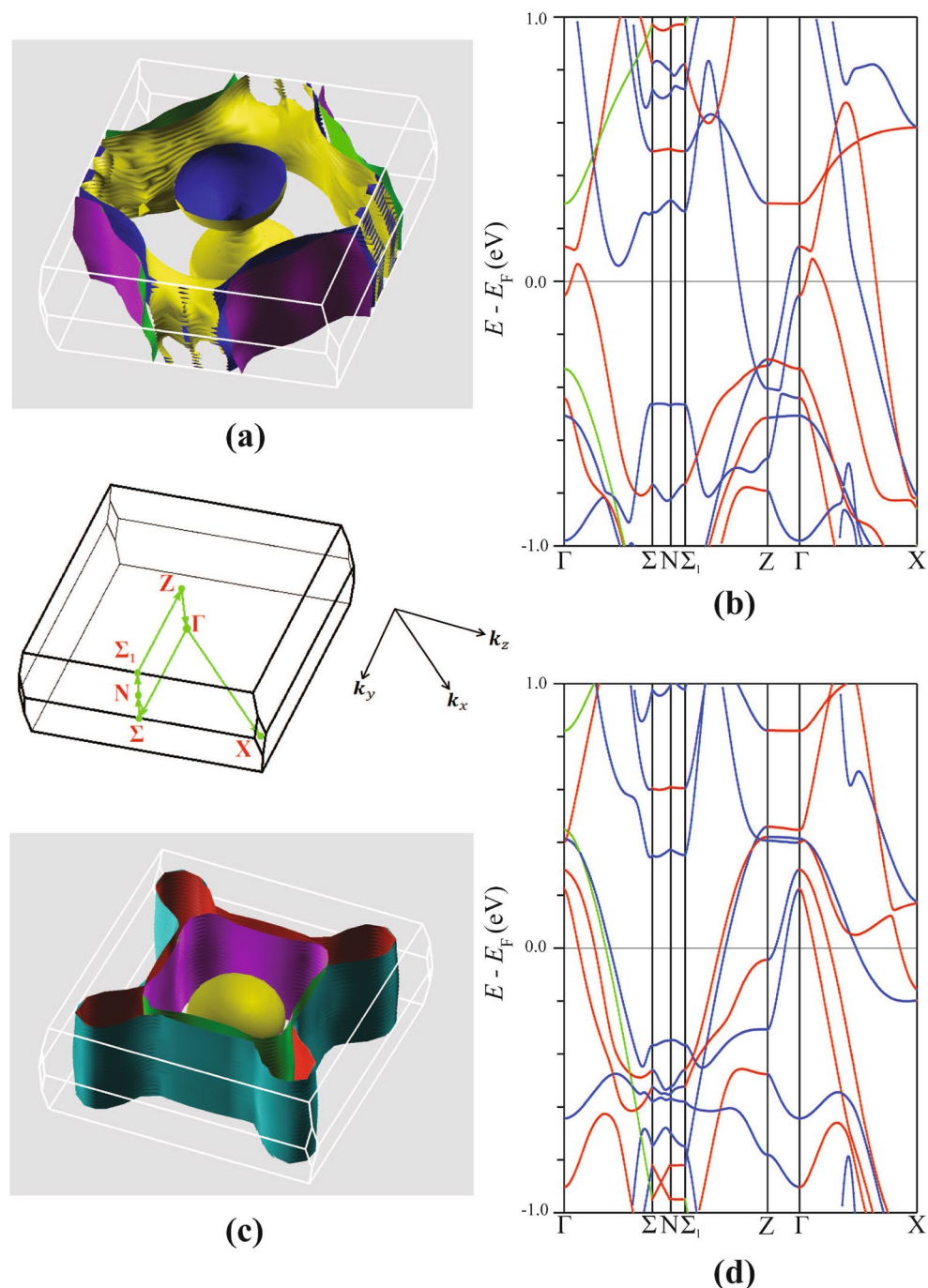


Figure 10. Spin-up (a) and spin-down (c) Fermi surfaces of EuFeAs_2 . The corresponding near-Fermi energy band structure for spin-up (b) and spin-down (d) energy bands. The corresponding \mathbf{k} -path traversed in the primitive Brillouin zone is shown at the center of the figure. SigmaPlot v14, www.systatsoftware.com.

There are three major contributions^{33,34} to the measured H_{hf} : the Fermi contact term H_c , the magnetic dipolar term H_{dip} , and the orbital moment term H_{orb} . Usually, the magnitude of the first term is much greater than that of the other two terms. The first term can be calculated from the following expression: $H_c = \frac{8\pi}{3} \mu_B^2 (\rho_{\uparrow}(0) - \rho_{\downarrow}(0))$. Here, $\rho_{\uparrow}(0)$ and $\rho_{\downarrow}(0)$ are the spin-up and spin-down densities at the Mössbauer nucleus, respectively. The calculated magnitudes of H_c at the ^{57}Fe and ^{151}Eu nuclei are, respectively, 59.8 and 308.7 kOe. These compare well with the corresponding experimental values (at 0 K) of 47.6(9) and 294.2(7) kOe⁹.

And finally, the calculated V_{zz} at the ^{151}Eu nuclei is $-5.54 \times 10^{21} \text{ V/m}^2$. It is in good agreement with the experimental value of $-4.98 \times 10^{21} \text{ V/m}^2$.

| Element | Magnetic moment |
|---------------------|-----------------|
| Eu | 6.90059 |
| As ₁ | − 0.07118 |
| As ₂ | − 0.02881 |
| As ₃ | − 0.02892 |
| Fe | 0.78029 |
| Muffin-tin region | 15.16166 |
| Interstitial region | 0.27656 |
| Total | 15.43822 |

Table 3. Calculated magnetic moments (in μ_B).

Conclusions

We performed a comprehensive first-principles study, using density-functional theory, of a new iron-pnictide compound EuFeAs₂. The geometry of the crystal structure and the atomic species in EuFeAs₂ lead to an interconnected network of Fe and As layers. These layers are separated by sheets of As atoms and insulating layers of Eu atoms. The calculated valence charge density maps show the existence of a mixture of ionic bonds between the Eu²⁺ and [FeAs₂]^{2−} ions, covalent bonds between the Fe and As₁ atoms, and directional bonds within the zigzag chains between the As₂ by As₃ atoms. The role of the Fe 3d orbitals in forming the band structure is discussed in detail. The band-structure similarities between EuFeAs₂ and other iron-based pnictides, as well as the unique band-structure features of EuFeAs₂, are elucidated. The 2D magnetism of EuFeAs₂ is shown to result from the spatial distribution of atoms. The magnetic moments of EuFeAs₂ and each constituent atom are calculated. We show that the calculated Mössbauer hyperfine-interaction parameters are in good agreement with the experimental ones.

Received: 8 January 2021; Accepted: 24 May 2021

Published online: 08 June 2021

References

- Katayama, N. *et al.* Superconductivity in Ca_{1-x}La_xFeAs₂: A novel 112-type iron pnictide with arsenic zigzag bonds. *J. Phys. Soc. Jpn.* **82**, 123702 (2013).
- Yakita, H. *et al.* A new layered iron arsenide superconductor: (Ca, Pr)FeAs₂. *J. Am. Chem. Soc.* **136**, 846 (2014).
- Kudo, K. *et al.* Enhanced superconductivity up to 43 K by P/Sb doping by P/Sb of Ca_{1-x}La_xFeAs₂. *J. Phys. Soc. Jpn.* **83**, 025001 (2014).
- Sala, A. *et al.* Synthesis and physical properties of Ca_{1-x}RE_xFeAs₂ with RE = La-Gd. *Appl. Phys. Express* **7**, 073102 (2014).
- Kudo, K. *et al.* Superconducting transition temperature of up to 47 K from simultaneous rare-earth element and antimony doping of 112-type CaFeAs₂. *J. Phys. Soc. Jpn.* **83**, 093705 (2014).
- Yu, J. *et al.* Discovery of a novel 112-type iron-pnictide and La-doping induced superconductivity in Eu_{1-x}La_xFeAs₂ (x = 0–0.15). *Sci. Bull.* **62**, 218 (2017).
- Yu, J. *et al.* Single crystal growth and characterization of the 112-type iron-pnictide EuFeAs₂. *Acta Phys. Sin.* **67**, 207403 (2018).
- Liu, Y.-B., Liu, Y., Jiao, W.-H., Ren, Z. & Cao, G.-H. Magnetism and superconductivity in Eu(Fe_{1-x}Ni_x)As₂ (x = 0, 0.04). *Sci. China-Phys. Mech. Astron.* **61**, 127405 (2018).
- Albedah, M. A., Stadnik, Z. M., Fedoryk, O., Liu, Y.-B. & Cao, G.-H. Magnetic properties of EuFeAs₂ and the 14 K superconductor EuFe_{0.97}Ni_{0.03}As₂. *J. Magn. Magn. Mater.* **503**, 166603 (2020).
- Liu, Z.-H. *et al.* Electronic structure of (Ca_{0.85}La_{0.15})FeAs₂. *Appl. Phys. Lett.* **106**, 052602 (2015).
- Liu, X. *et al.* Fermi surface and band structure of (Ca, La)FeAs₂ superconductor from angle-resolved photoemission spectroscopy. *Chin. Phys. Lett.* **30**, 127402 (2013).
- Jiang, S. *et al.* Structural and magnetic phase transitions in Ca_{0.73}La_{0.27}FeAs₂ with electron-overdoped FeAs layers. *Phys. Rev. B* **93**, 054522 (2016).
- Li, M. Y. *et al.* Significant contribution of As 4p orbitals to the low-lying electronic structure of the 112-type iron-based superconductor Ca_{0.9}La_{0.1}FeAs₂. *Phys. Rev. B* **91**, 045112 (2015).
- Kang, C.-J., Birol, T. & Kotliar, G. Phase stability and large in-plane resistivity anisotropy in the 112-type iron-based superconductor Ca_{1-x}La_xFeAs₂. *Phys. Rev. B* **95**, 014511 (2017).
- P. Blaha, K. Schwartz, G. Madsen, D. Kvasnicka, and J. Luitz. *WIEN2k, An Augmented Plane Wave Plus Local Orbitals Program for Calculating Crystal Properties* (Karlheinz Schwarz, Technical Universität Wien, Austria, 1999).
- Nejadsattari, F., Wang, P., Stadnik, Z. M., Nagata, Y. & Ohnishi, T. *Ab-initio*, and ¹⁵⁵Gd Mössbauer spectroscopy study of GdRhO₃. *J. Alloys Compd.* **725**, 1098 (2017).
- Perdew, J. P., Burke, S. & Ernzerhof, M. Generalized gradient approximation made simple. *Phys. Rev. Lett.* **77**, 3865 (1996).
- Madsen, G. K. H. & Novák, P. Charge order in magnetite. An LDA+U study. *Europhys. Lett.* **69**, 777 (2005).
- Kreyssig, A. *et al.* Pressure-induced volume-collapsed tetragonal phase of CaFe₂As₂ as seen via neutron scattering. *Phys. Rev. B* **78**, 184517 (2008).
- Rutzinger, D. *et al.* Lattice distortions in layered type arsenides LnTAs₂ (Ln = La-Nd, Sm, Gd, Tb; T = Ag, Au): Crystal structures, electronic and magnetic properties. *J. Solid State Chem.* **183**, 510 (2010).
- Bader, R. F. W. *Atoms in Molecules: A Quantum Theory* (Oxford University Press, 1991).
- F. Grandjean & G. L. Long. in *Mössbauer Spectroscopy Applied to Inorganic Chemistry*, Vol. 3, 513 (eds. G. J. Long & F. Grandjean). (Plenum, 1989).
- Blöchl, P. E., Jepsen, O. & Andersen, O. K. Improved tetrahedron method for Brillouin-zone integrations. *Phys. Rev. B* **49**, 16223 (1994).
- Nejadsattari, F., Albedah, M. A. & Stadnik, Z. M. Electronic structure and magnetism of the 35 K superconductor CsEuFe₄As₄. *J. Phys. Chem. Solids* **136**, 109137 (2020).

25. Nejadstari, F., Albedah, M. A. & Stadnik, Z. M. *Ab-initio* study of the RbEuFe₄As₄ superconductor. *Philos. Mag.* **100**, 894 (2020).
26. Singh, D. J. Electronic structure of Fe-based superconductors. *Physica C* **469**, 418 (2009).
27. Ding, H. *et al.* Electronic structure of optimally doped pnictide Ba_{0.6}K_{0.4}Fe₂As₂: A comprehensive angle-resolved photoemission spectroscopy investigation. *J. Phys. Condens. Matter* **23**, 135701 (2011).
28. Craco, L., Laad, M. S., Leoni, S. & Rosner, H. Normal-state correlated electronic structure of iron pnictides from first principles. *Phys. Rev. B* **78**, 134511 (2008).
29. Han, M. J., Yin, Q., Pickett, W. E. & Savrasov, S. Y. Anisotropy, itineracy, and magnetic frustration in high-*T_C* iron pnictides. *Phys. Rev. Lett.* **102**, 107003 (2009).
30. Mazin, I., Shimizu, M., Takemori, N. & Jeschke, H. O. Novel Fe-based superconductor LaFe₂As₂ in comparison with traditional pnictides. *Phys. Rev. Lett.* **123**, 267001 (2019).
31. Shim, H., Haule, K. & Kotliar, G. Density-functional calculations of the electronic structures and magnetism of the pnictide superconductors BaFeAs₂ and BaFeSb₂. *Phys. Rev. B* **79**, 060501(R) (2009).
32. Li, W., Zhu, J.-X., Chen, Y. & Ting, C. S. First-principles calculations of the electronic structure of iron-pnictide EuFe₂(As, P)₂ superconductors: Evidence for antiferromagnetic spin order. *Phys. Rev. B* **86**, 155119 (2012).
33. Greenwood, N. N. & Gibb, T. C. *Mössbauer Spectroscopy* (Chapman and Hall, 1971).
34. Gütlich, P., Bill, E. & Trautwein, A. *Mössbauer Spectroscopy and Transition Metal Chemistry* (Springer, 2011).
35. Nejadstari, F., Stadnik, Z. M. & Zukrowski, J. Mössbauer spectroscopy study of a new layered iron oxyselenide Na₂Fe₂Se₂O. *J. Alloys Compd.* **639**, 547 (2015).
36. Wdowik, U. D. & Reubenbauer, K. Calibration of the isomer shift for the 14.4-keV transition in ⁵⁷Fe using the full-potential linearized augmented plane-wave method. *Phys. Rev. B* **76**, 155118 (2007).

Acknowledgements

This work was supported by the Natural Sciences and Engineering Research Council of Canada.

Author contributions

F.N. and Z.M.S. wrote the main manuscript text and reviewed it.

Competing interests

The authors declare no competing interests.

Additional information

Correspondence and requests for materials should be addressed to Z.M.S.

Reprints and permissions information is available at www.nature.com/reprints.

Publisher's note Springer Nature remains neutral with regard to jurisdictional claims in published maps and institutional affiliations.



Open Access This article is licensed under a Creative Commons Attribution 4.0 International License, which permits use, sharing, adaptation, distribution and reproduction in any medium or format, as long as you give appropriate credit to the original author(s) and the source, provide a link to the Creative Commons licence, and indicate if changes were made. The images or other third party material in this article are included in the article's Creative Commons licence, unless indicated otherwise in a credit line to the material. If material is not included in the article's Creative Commons licence and your intended use is not permitted by statutory regulation or exceeds the permitted use, you will need to obtain permission directly from the copyright holder. To view a copy of this licence, visit <http://creativecommons.org/licenses/by/4.0/>.

© The Author(s) 2021